

Strain effects in monolayer Iron-Chalcogenide superconductors

Cesare Tresca¹, Fabio Ricci^{2,3} and Gianni Profeta^{1,2}

¹ *Dipartimento di Scienze Fisiche e Chimiche, Università dell'Aquila, 67100 Coppito (L'Aquila), Italy*

² *Consiglio Nazionale delle Ricerche, Istituto Superconduttori,*

Materiali Innovativi e Dispositivi (CNR-SPIN), 67100 L'Aquila, Italy and

³ *Physique Théorique des Matériaux, Université de Liège (B5), B-4000 Liège, Belgique*

The successful fabrication of one monolayer FeSe on SrTiO₃ represented a real breakthrough in searching for high-T_c Fe-based superconductors (Ref.¹). Motivated by this important discovery, we studied the effects of tensile strain on one monolayer and bulk iron-chalcogenide superconductors (FeSe and FeTe), showing that it produces important magnetic and electronic changes in the systems. We found that the magnetic ground state of bulk and monolayer FeSe is the block-checkerboard phase, which turns into the collinear stripe phase under in plane tensile strain. FeTe, in both bulk and monolayer phases, shows two magnetic transitions upon increasing the tensile strain: from bicollinear in the ground state to block-checkerboard ending up to the collinear antiferromagnetic phase which could bring it in the superconducting state. Finally, the study of the mechanical properties of both FeSe and FeTe monolayers reveals their enormous tensile strain limits and opens the possibility to grow them on different substrates.

Introduction

Since the discovery of high critical temperature superconductivity in fluorine doped iron arsenide LaFeAsO (T_c = 26 K)², the attention of the scientific community has been captured by Fe-based superconductors (FeSCs).

Among all FeSCs families known, the iron-chalcogenide (FeCh) (FeSe, FeTe, FeSe_xTe_{1-x}) family has a fundamental importance for the understanding of the structural, electronic, magnetic and superconducting properties of FeSCs³. In fact, thanks to their simple crystal structure, being composed by one layer of square Fe lattice tetrahedrally bonded to Ch (see Fig.1), FeCh can be thought as a fundamental building block of this class of materials and the perfect test case to study the superconducting mechanisms in these compounds.

FeSe superconducts at ambient conditions with T_c = 8 K, probably due to presence of Se vacancies⁴. On the contrary, FeTe is not superconductor, however, partial substitution of Te with Se allows superconductivity to emerge, reaching T_c ~ 15 K at the optimal substitution of 50%. The origin of the superconducting phase is commonly attributed to the developing of spin fluctuations with wave-vector $\mathbf{Q} = (\pi, \pi)$ (associated with a collinear antiferromagnetic stripe phase (AFM1) in which ferromagnetically ordered nearest-neighbouring Fe stripes are aligned perpendicularly to the antiferromagnetically ordered ones, see Fig.1)^{3,5}. In fact, despite the structural and electronic similarities with FeSe, FeTe shows a bicollinear antiferromagnetic phase (AFM2)⁶.

Structural properties are found to be strongly linked to the superconducting properties in these materials. Indeed, a strong enhancement of T_c up to 37 K is observed in FeSe at pressure near 9 GPa⁷. On the other hand, FeSe thin films under tensile strain of about 3.7% show the suppression of superconducting phase⁸. The role of the pressure and strain has been discovered to be of fundamental importance also in FeTe. Not only pressure does not induce superconductivity in FeTe, but favours a

ferromagnetic phase⁹. However, it was shown that FeTe thin films become superconductor at 13 K under tensile strain conditions¹⁰.

A turning point in the exploration of FeSCs was recently provided by the discovery that low dimensionality raises dramatically the superconducting critical temperature of FeSe¹. Recent experiments, in fact, show exciting properties of monolayer (ML) FeSe, with respect to the bulk phase. In particular, Meissner effect was observed at 20 K in few layer FeSe grown on SrTiO₃ (STO) substrate (lattice constant 3.90 Å)¹¹. Peng *et al.*¹² reported an enhancement of the superconducting critical temperature in the extremely expanded FeSe monolayer grown on Nb doped STO (lattice constant 3.99 Å) measuring a superconducting gap up to 70 K. There is direct observation of zero resistivity under 40 K in *ex-situ* experiments¹³ and ~ 109 K in the recent *in-situ* experiment with 4-point probe¹⁴.

All these results represent rather solid proofs that a superconducting phase exists indeed in FeSe ML.

The Fermi surface (FS) of monolayer FeSe, measured using *in situ* ARPES technique^{15,16} also as a function of the film thickness grown on STO¹⁷, reveals that it is characterized by only electron FS at *M* point of the Brillouin Zone (BZ), apparently losing the hole FS at Γ . Surprisingly, this is topologically different from the FS of the bilayer (and bulk) system, which shows the typical FeSC's FS composed by hole cylinders at the BZ center and electron features at the BZ corners¹⁷.

At the moment various mechanisms have been proposed to explain the high superconducting transition temperature of the FeSe ML. In particular, the electron-phonon coupling with oxygen optical phonons in STO which can induce a small momentum pairing further increasing the spin-fluctuation coupling¹⁸. The role of the substrate was also emphasized in Ref.¹⁹; here the authors suggest that the electron-phonon coupling in FeSe is enhanced by the presence of the substrate imposing both structural and magnetic constrains.

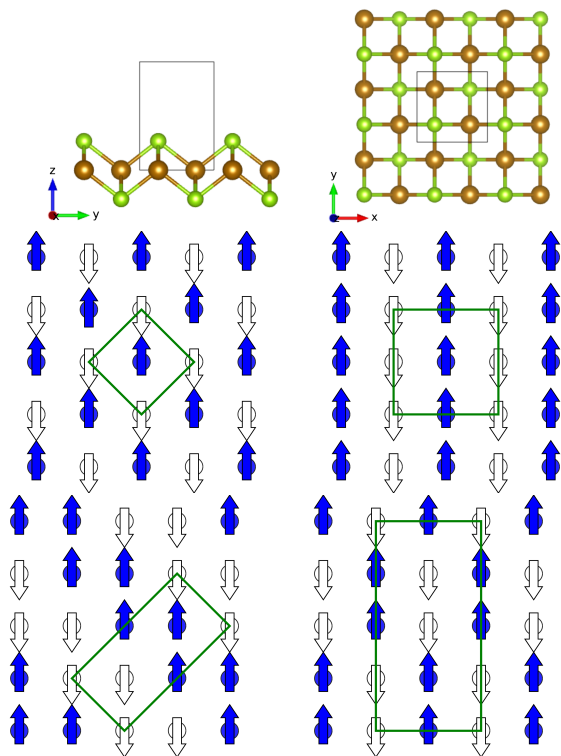


FIG. 1: Crystal structure of iron chalcogenides and magnetic phases considered. Upper panels: Side (left) and top (right) view of FeCh monolayer crystal. Large spheres indicate Fe atoms while smaller ones Ch atoms. The unit cell of the bulk phase is drawn as thin line and the directions of in-plane (\mathbf{a} and \mathbf{b}) and out-of-plane (\mathbf{c}) lattice vectors are highlighted. Lower panels, from left to right: AFM0, AFM1, AFM2 and AFM3 magnetic phases (see text) with the corresponding in plane unit cell.

Indeed, in these particular two dimensional (2D) conditions, an additional role can be played by the substrate and thus by epitaxial strain which may, also, suppress the magneto-elastic coupling.

Considering the reported sensitivity of the physical and superconducting properties of FeCh to structural conditions^{8,10}, in this paper we studied by first principles density functional theory (DFT) the effect of strain on the structural, magnetic and electronic properties of FeSe and FeTe in both ML and bulk phases with the aim of understanding the origin of the enhancement (or of the suppression) of the superconducting phase.

I. COMPUTATIONAL DETAILS

Calculations were performed using the Vienna Ab-initio Simulation Package (VASP)^{20,21}, using the Generalized Gradient Approximation (GGA)²² to the exchange-correlation energy. Van der Waals interactions, not negligible in FeCh systems²³, were included as dispersive term, using the DFT-D2 Grimme's semi-empirical

correction^{24,25}.

We studied the strain effects considering different magnetic phases (see below). In order to simulate the structural effects of the STO substrate (which constrains the in-plane lattice constants), we neglected the in-plane magneto-elastic distortion. Once the ground state geometry for each system was determined including magnetic distortions with inequivalent \mathbf{a} and \mathbf{b} directions, the systems were constrained to in-plane lattice constants $a = (|\mathbf{a}| + |\mathbf{b}|)/2$: this is assumed to be the reference system in the *un-strained* condition. Strain effects were studied calculating the total energy as a function of the applied in-plane strain (varying the a in-plane lattice constant) considering different competing magnetic phases (schematically shown in Fig.1): the checkerboard order of the iron spin (called AFM0), the collinear stripe phase (AFM1), the bi-collinear one (AFM2) and the recently proposed block-checkerboard order (AFM3)²⁶. The magnetic order along the out-of-plane axis is considered ferromagnetic for all the bulk phases. We used Projected Augmented-Wave pseudopotentials²⁷ for all the atomic species involved, with an energy cutoff of 350 eV. Integration over BZ was performed using different uniform Monkhorst and Pack grids²⁸ depending on the lattice: $16 \times 16 \times 10$ for the tetragonal ($a \times a \times c$) non magnetic (NM) phase (containing two Fe and two Ch atoms), $8 \times 8 \times 10$ for magnetic cell ($2a \times 2a \times c$) commensurate to the AFM0, AFM1 and AFM2 magnetic phases. The AFM3 phase was simulated using $\sqrt{2}a \times 2\sqrt{2}a \times c$ unit cell using a Monkhorst and Pack grid of $8 \times 4 \times 10$. For the ML systems we considered a supercell including ~ 10 Å of vacuum. Using these parameters the total energy of the considered systems are converged to less than 0.1 meV/atom.

The calculations of band structures and FS's have been performed using the NM electronic states²⁹.

II. RESULTS AND DISCUSSION

The total energy of FeSe ML as a function of the in-plane lattice constant for the lowest energy magnetic structures are shown in Fig. 2(a). At variance with what was expected in line with the collinear stripe ground state of pnictides, the ground state magnetic order is the block-checkerboard with equilibrium structural parameters reported in Tab. I. Similar with what found in the AFM1 phase, the magneto-elastic coupling causes the inequivalence of \mathbf{a} and \mathbf{b} directions.

The magnetic moment of Fe atoms in the monolayer phase is $0.2 \mu_B$ higher with respect to the bulk system (see Table I) and changes slightly (less than $0.1 \mu_B$) depending on the magnetic order.

Fig.2(a) shows that the AFM1 phase is the more stable phase under applied in-plane strain, which induces a magnetic phase transition at $a \simeq 3.9$ Å. Considering that the superconducting pairing could be mediated by (π, π) spin-fluctuations, free-standing stoichiometric

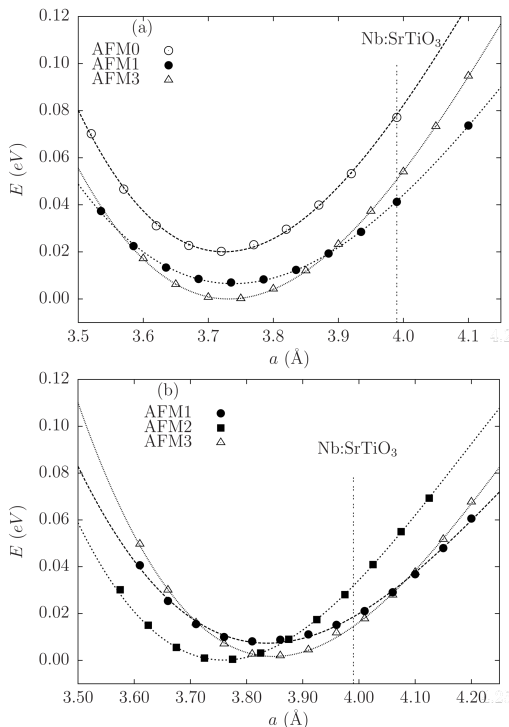


FIG. 2: Total energy per atom as a function of the in-plane lattice parameter for ML FeSe (panel (a)) and FeTe (panel (b)). The theoretical points are fitted with a cubic function. The dotted vertical line indicates the Nb:SrTiO₃ lattice parameter (see text).

FeSe monolayer with a $(\pi, \pi/2)$ magnetic order is not expected to be superconductor, however it may support a superconducting phase if strained at the STO lattice constant in agreement with experimental evidences¹². The AFM1 phase increases its stability under applied strain and becomes the ground state at the Nb:SrTiO₃ lattice constant (see Fig.2(a)) where experiments report the highest critical temperature¹².

	FeSe	FeTe
$ \mathbf{a} $ (Å)	3.75	4.04
$ \mathbf{b} $ (Å)	3.72	3.51
h_{ch} (Å)	1.44	1.79
$ m $ (μ_B)	2.1	2.5

TABLE I: Equilibrium structural parameters of FeSe and FeTe ML in their respective ground state ($|\mathbf{a}|$ and $|\mathbf{b}|$ lattice constants and the height of the chalcogenide, h_{ch}) and Fe magnetic moment, $|m|$.

The variation of about 6% of the in-plane lattice constant (Nb:SrTiO₃) determines a strong effect on the FS, as reported in Fig. 3. This is mainly due to the contraction of the Se height from the Fe plane, h_{ch} (Fig.1), which moves from 1.44 Å (equilibrium geometry) to 1.34 Å at the in-plane lattice constant of Nb:SrTiO₃. In the free-standing ML, there are three hole-type FS's at the Γ

point and two (quasi overlapping) electron-like FS's at the BZ corner (Fig. 3(a)). Stretching the FeSe ML at the Nb:SrTiO₃ lattice parameter (Fig. 3(b)) fills completely the $d_{x^2-y^2}$ hole-type band near Γ and makes the corresponding FS to vanish. At the same time, the electron FS's change their shape and shrink as a result of electron counting. ARPES measurements, however, seem to find a different scenario¹⁷: only electron sheets at the BZ corner are found with no evidences of hole-type FS at the BZ center.

Although the calculated electronic properties do not completely agree with available experiments, we indeed predict that strain induces a magnetic phase transition and a subsequent topological transition in the FS of the ML phase of FeSe.

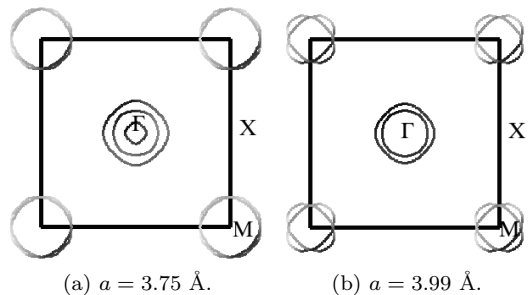


FIG. 3: Fermi surface of FeSe at equilibrium (a) and strained at Nb:SrTiO₃ lattice parameter (b).

We now consider the monolayer phase of FeTe, a system not yet experimentally realized. As already discussed, bulk FeTe is not superconducting, however the effect of the in-plane strain has been shown to induce a superconducting phase with a critical temperature of 13 K¹⁰. In principle, a monolayer of FeTe can result more interesting than the FeSe monolayer; in fact, if superconductivity is mediated by spin-fluctuations, FeTe is expected to have a stronger pairing³⁰.

The ground state of FeTe ML is found to be AFM2 with lattice parameters reported in Tab. I. While the magnetic induced distortion of the square lattice is minimal in FeSe, in FeTe it is sensible. In addition, the magnetic moment of Fe atoms is larger in the ground state (AFM2) of FeTe than in FeSe (see Table I) and shows a reduction of $0.3\mu_B$ in the AFM1 phase. From Fig. 2(b) we note that two magnetic phase transitions take place as a function of the tensile strain: from AFM2 to AFM3 at $a \gtrsim 3.80$ Å and from AFM3 to AFM1 at $a \gtrsim 4.05$ Å.

The FS's shape of FeTe ML changes from the equilibrium (Fig.4(a)) to the strained phase (Fig. 4(b)). In this last geometry, the FS shows two hole pockets at Γ and two (quasi overlapping) electron features at M nearly nested with $\mathbf{Q} = (\pi, \pi)$. Therefore the magnetic transition towards the AFM1 phase with this ordering vector allows the pairing between hole and electron FS's sheets which was hindered in the bicollinear and block-

checkerboard phases. Based on these structural, magnetic and electronic properties we propose strained FeTe ML as a good candidate for interesting superconducting properties, potentially better than FeSe ML.

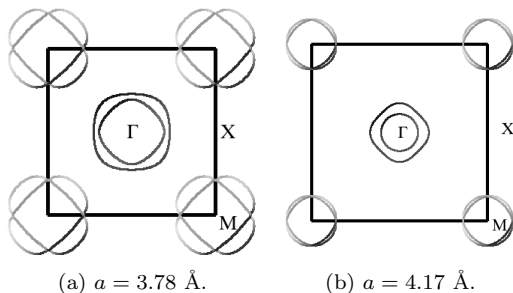


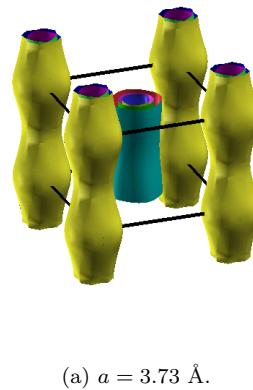
FIG. 4: Fermi surface for FeTe ML at equilibrium (panel a) and strained at 4.17 Å in-plane lattice parameter (panel b).

The results obtained in the monolayer systems help the interpretation of the effects of in-plane strain on the superconducting properties of FeCh bulk systems. Indeed, for FeSe and FeTe thin films a different behaviour under tensile strain was experimentally reported. FeSe grown on STO shows suppression of the superconducting phase observed on unstrained compounds⁸, while, bulk FeTe becomes superconductor upon the same tensile strain conditions¹⁰.

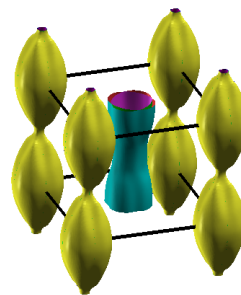
Total energy calculations performed constraining the in-plane lattice parameter and fully relaxing all the others (*i.e.* out-of-plane axis and internal positions) show that the magnetic ground state of bulk FeSe at equilibrium is the AFM3 order, and it becomes AFM1 at the Nb:STO in-plane lattice constant. Thus, suppression of the superconducting state in strained FeSe^{8,31} can be interpreted considering that strain causes a topological transition leading to a complete closure of the electron FS cylinders at M (present at the equilibrium, see Fig.5(a)). At $a \gtrsim 3.99$ Å the FS becomes three dimensional (see Fig. 5(b)), strongly reducing the pairing.

On the contrary, we find that FeTe bulk has a bi-collinear (AFM2) magnetic ground state in agreement with experiments³². However, a transition towards the AFM3 phase takes place at $a \simeq 3.8$ Å; upon further increase of the tensile strain above $a \gtrsim 4.10$ Å, the system develops an AFM1 ground state. In this last phase, bulk FeTe preserves both hole and electron sheets although with sensible differences with respect to the equilibrium phase (Fig.6). On the basis of these results, the experimental evidences reported by Han *et al.*¹⁰ find now a natural interpretation: strain causes AFM1 spin-fluctuations which couple the hole and electron FS sheets via the AFM1 \mathbf{Q} vector.

In order to possibly guide new experiments towards the use of alternative substrates to properly tune strain conditions in both bulk and monolayer systems, we investigated the mechanical properties of FeSe and FeTe



(a) $a = 3.73$ Å.



(b) $a = 3.99$ Å.

FIG. 5: Fermi surface for FeSe bulk at equilibrium (panel (a)) and strained at Nb:STO lattice parameter (panel (b)). The Γ -point is the center of the first BZ shown as thin lines.

ML to obtain information on the stiffness and breaking strength of these compounds. Starting from the equilibrium structure, we studied the stress-strain relation for FeSe and FeTe ML and report the results in Fig. 7. Here, the tensile strain is defined as $\varepsilon = (\varepsilon_{xx} + \varepsilon_{yy})/\sqrt{2}$ with $\varepsilon_{xx} = (a' - a)/a$ and $\varepsilon_{yy} = (b' - b)/b$ ³³, being a and b the lattice parameters along \hat{x} and \hat{y} directions respectively³⁴.

The stress-strain curve for FeSe and FeTe shows a maximum at the critical strain of $\varepsilon = 0.33$ and $\varepsilon = 0.39$, respectively. Although the corresponding maximal stress ($\sigma_{max}^{FeSe} = 11.9$ GPa and $\sigma_{max}^{FeTe} = 9.1$ GPa) is very low compared to other monolayers as graphene or dichalcogenides (*i.e.* MoS₂), these results demonstrate that both compounds can support relevant strain, comparable with what recently found for phosphorene³⁵. This can open the way to future growth of superconducting chalcogenides on different substrates with quite large mismatch.

III. CONCLUSIONS

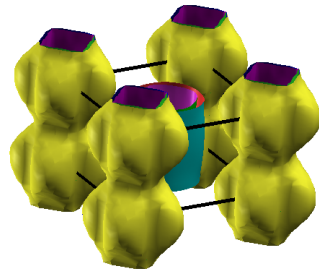
Using first-principles DFT simulations we calculated the mechanical, electronic and magnetic properties of FeCh in 2D and bulk geometries under in-plane strain. Our predictions show that:

(i) The magnetic ground state of monolayer and bulk FeSe is the block-checkerboard. Application of tensile strain produces a magnetic transition towards the AFM1 phase with the closure of only one FS at the Γ point in FeSe ML.

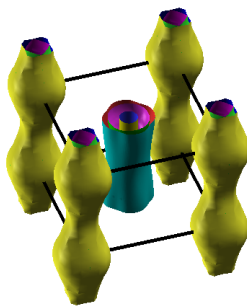
In the bulk geometry, strain induces a topological transition of the FS at M , that can be at the origin of the suppression of the superconducting state.

(ii) If FeTe ML could be strained above 9%, it will achieve all the requirements needed to observe a superconducting transition: AFM1 magnetic ground state with hole and electron FS's sheets nested with the proper ordering wave vector. The same effect is predicted also in the bulk phase as well.

(iii) Both FeSe and FeTe ML have large enough mechanical flexibility to support critical strains up to $\varepsilon \gtrsim 30\%$.



(a) $a = 3.75 \text{ \AA}$.



(b) $a = 4.10 \text{ \AA}$.

FIG. 6: Fermi surface for FeTe bulk at equilibrium (panel (a)) and strained at 4.10 \AA lattice parameter (panel (b)). The Γ -point is the center of the first BZ shown as thin lines.

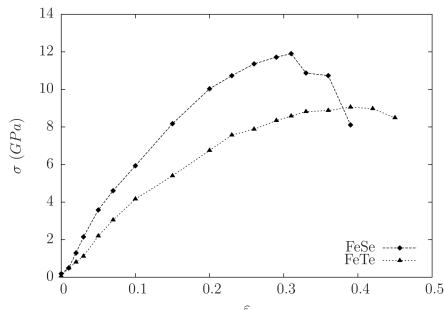


FIG. 7: Stress-strain relation for FeSe and FeTe ML.

IV. ACKNOWLEDGMENTS

We thank Prof. L. Ottaviano for stimulating discussions and for valuable editing contribution and Prof. A. Continenza for critically reading the manuscript. This work was supported by FP7 European project SUPER-IRON (grant agreement No. 283204) and by the Italian Ministry of University Research through the PRIN 2012 project. We also acknowledge the CINECA award under the ISCRA initiative, for access to high performance computing resources and support.

¹ Qing-Yan W, Zhi L, Wen-Hao Z, Zuo-Cheng Z, Jin-Song Z, Wei L, Hao D, Yun-Bo O, Peng D, Kai C, Jing W, Can-Li S, Ke H, Jin-Feng J, Shuai-Hua J, Ya-Yu W, Li-Li W, Xi C, Xu-Cun M and Qi-Kun X 2012 *Chinese Physics Letters* **29** 037402 URL [http://stacks.iop.org/0256-307X/29/](http://stacks.iop.org/0256-307X/29/i=3/a=037402)

² Kamihara Y, Watanabe T, Hirano M and Hosono H 2008 *Journal of the American Chemical Society* **130** 3296–3297 (*Preprint* <http://pubs.acs.org/doi/pdf/10.1021/ja800073m>) URL

- <http://pubs.acs.org/doi/abs/10.1021/ja800073m>
- ³ Paglione J and Greene R L 2010 *Nat. Phys.* **6**(9) 645–658 URL <http://dx.doi.org/10.1038/nphys1759>
 - ⁴ Hsu F and *et. al.* 2008 *Proceedings of the National Academy of Sciences* **105** 14262
 - ⁵ Wang F and Lee D H 2011 *Science* **332** 200–204 (*Preprint* <http://www.sciencemag.org/content/332/6026/200.full.pdf>) URL <http://www.sciencemag.org/content/332/6026/200.abstract>
 - ⁶ Mizuguchi Y and Takano Y 2011 *Zeitschrift für Kristallographie Crystalline Materials* **226** 417–434
 - ⁷ Medvedev S and *et. al.* 2009 *Nature Materials* **8**(8) 630 URL <http://dx.doi.org/10.1038/nmat2491>
 - ⁸ Nie Y F, Brahim E, Budnick J I, Hines W A, Jain M and Wells B O 2009 *Applied Physics Letters* **94** 242505 URL <http://scitation.aip.org/content/aip/journal/apl/94/24/10.1063/1.3155441>
 - ⁹ Monni M, Bernardini F, Profeta G and Massidda S 2013 *Phys. Rev. B* **87**(9) 094516 URL <http://link.aps.org/doi/10.1103/PhysRevB.87.094516>
 - ¹⁰ Han Y, Li W Y, Cao L X, Wang X Y, Xu B, Zhao B R, Guo Y Q and Yang J L 2010 *Phys. Rev. Lett.* **104**(1) 017003 URL <http://link.aps.org/doi/10.1103/PhysRevLett.104.017003>
 - ¹¹ Deng L Z, Lv B, Wu Z, Xue Y Y, Zhang W H, Li F H, Wang L L, Ma X C, Xue Q K and Chu C W 2013 *ArXiv e-prints (Preprint 1311.6459)*
 - ¹² Peng R, Shen X P, Xie X, Xu H C, Tan S Y, Xia M, Zhang T, Cao H Y, Gong X G, Hu J P, Xie B P and Feng D L 2014 *Phys. Rev. Lett.* **112**(10) 107001 URL <http://link.aps.org/doi/10.1103/PhysRevLett.112.107001>
 - ¹³ Zhang W H, Sun Y, Zhang J S, Li F S, Guo M H, Zhao Y F, Zhang H M, Peng J P, Xing Y, Wang H C, Fujita T, Hirata A, Li Z, Ding H, Tang C J, Wang M, Wang Q Y, He K, Ji S H, Chen X, Wang J F, Xia Z C, Li L, Wang Y Y, Wang J, Wang L L, Chen M W, Xue Q K and Ma X C 2014 *Chinese Physics Letters* **31** 017401 (*Preprint 1311.5370*)
 - ¹⁴ Ge J F, Liu Z L, Liu C, Gao C L, Qian D, Xue Q K, Liu Y and Jia J F 2014 *ArXiv e-prints (Preprint 1406.3435)*
 - ¹⁵ Liu D, Zhang W, Mou D, He J, Ou Y B, Wang Q Y, Li Z, Wang L, Zhao L, He S, Peng Y, Liu X, Chen C, Yu L, Liu G, Dong X, Zhang J, Chen C, Xu Z, Hu J, Chen X, Ma X, Xue Q and Zhou X 2012 *Nature Communications* **3** 931
 - ¹⁶ He S, He J, Zhang W, Zhao L, Liu D, Liu X, Mou D, Ou Y B, Wang Q Y, Li Z, Wang L, Peng Y, Liu Y, Chen C, Yu L, Liu G, Dong X, Zhang J, Chen C, Xu Z, Chen X, Ma X, Xue Q and Zhou X J 2013 *Nature Materials* **12** 605
 - ¹⁷ Tan S, Zhang Y, Xia M, Ye Z, Chen F, Xie X, Peng R, Xu D, Fan Q, Xu H, Jiang J, Zhang T, Lai X, Xiang T, Hu J, Xie B and Feng D 2013 *Nature Materials* **12**(7) 634 URL <http://dx.doi.org/10.1038/nmat3654>
 - ¹⁸ Lee J J, Schmitt F T, Moore R G, Johnston S, Cui Y T, Li W, Yi M, Liu Z K, Hashimoto M, Zhang Y, Lu D H, Devereaux T P, Lee D H and Shen Z X 2014 *Nature* **515** 245
 - ¹⁹ Coh S, Cohen M L and Louie S G 2014 *ArXiv e-prints (Preprint 1407.5657)*
 - ²⁰ Kresse G and Furthmüller J 1996 *Phys. Rev. B* **54**(16) 11169–11186 URL <http://link.aps.org/doi/10.1103/PhysRevB.54.11169>
 - ²¹ Kresse G and Furthmüller J 1996 *Computational Materials Science* **6** 15 – 50 ISSN 0927-0256 URL <http://www.sciencedirect.com/science/article/pii/0927025696000080>
 - ²² Kresse G and Joubert D 1999 *Phys. Rev. B* **59**(3) 1758–1775 URL <http://link.aps.org/doi/10.1103/PhysRevB.59.1758>
 - ²³ Ricci F and Profeta G 2013 *Phys. Rev. B* **87**(18) 184105 URL <http://link.aps.org/doi/10.1103/PhysRevB.87.184105>
 - ²⁴ Grimme S 2006 *Journal of Computational Chemistry* **27** 1787–1799 ISSN 1096-987X URL <http://dx.doi.org/10.1002/jcc.20495>
 - ²⁵ We considered the equilibrium structure obtained considering the vdW correction only for the out-of-plane lattice constants (see also Ref.²³).
 - ²⁶ Cao H Y, Chen S, Xiang H and Gong X G 2014 *ArXiv e-prints (Preprint 1407.7145)*
 - ²⁷ Blöchl P E 1994 *Phys. Rev. B* **50**(24) 17953–17979 URL <http://link.aps.org/doi/10.1103/PhysRevB.50.17953>
 - ²⁸ Monkhorst H J and Pack J D 1976 *Phys. Rev. B* **13**(12) 5188–5192 URL <http://link.aps.org/doi/10.1103/PhysRevB.13.5188>
 - ²⁹ Colonna N, Profeta G, Continenza A and Massidda S 2011 *Phys. Rev. B* **83**(9) 094529 URL <http://link.aps.org/doi/10.1103/PhysRevB.83.094529>
 - ³⁰ Subedi A, Zhang L, Singh D J and Du M H 2008 *Phys. Rev. B* **78**(13) 134514 URL <http://link.aps.org/doi/10.1103/PhysRevB.78.134514>
 - ³¹ Winiarski M J, Samsel-Czekala M and Ciechan A 2012 *EPL (Europhysics Letters)* **100** 47005 URL <http://stacks.iop.org/0295-5075/100/i=4/a=47005>
 - ³² Bao W, Qiu Y, Huang Q, Green M A, Zajdel P, Fitzsimmons M R, Zhernenkov M, Chang S, Fang M, Qian B, Vohstedt E K, Yang J, Pham H M, Spinu L and Mao Z Q 2009 *Phys. Rev. Lett.* **102**(24) 247001 URL <http://link.aps.org/doi/10.1103/PhysRevLett.102.247001>
 - ³³ Isaacs E B and Marianetti C A 2014 *Phys. Rev. B* **89**(18) 184111 URL <http://link.aps.org/doi/10.1103/PhysRevB.89.184111>
 - ³⁴ In order to calculate the stress in 2D, we divided the computed 3D stress by a factor c/d_0 , where c is the lattice vector of the supercell used in simulation and d_0 is the distance between the Fe planes in the corresponding bulk system.
 - ³⁵ Wei Q and Peng X 2014 *ArXiv e-prints* URL <http://adsabs.harvard.edu/abs/2014arXiv1403.7882W>